Liquid Crystals
Publication details, including instructions for authors and subscription information:
http://www.informaworld.com/smpp/title~content=t713926090

Polymorphism, crystal-crystal and liquid crystalline thermotropic phase transition behaviour of even chain length zinc(II) *n*-alkanoates

Richard A. Taylor[a]; Henry A. Ellis[b]
[a] Department of Chemistry, Faculty of Science and Agriculture, University of the West Indies, St. Augustine, Trinidad and Tobago, West Indies [b] Department of Chemistry, Faculty of Pure and Applied Sciences, University of the West Indies, Jamaica, West Indies

To cite this Article Taylor, Richard A. and Ellis, Henry A.(2009) 'Polymorphism, crystal-crystal and liquid crystalline thermotropic phase transition behaviour of even chain length zinc(II) *n*-alkanoates', Liquid Crystals, 36: 3, 257 — 268
To link to this Article: DOI: 10.1080/02678290902842594
URL: http://dx.doi.org/10.1080/02678290902842594

Liquid Crystals,
Vol. 36, No. 3, March 2009, 257–268

Taylor & Francis
Taylor & Francis Group

Polymorphism, crystal–crystal and liquid crystalline thermotropic phase transition behaviour of even chain length zinc(II) *n*-alkanoates

Richard A. Taylor[a]* and Henry A. Ellis[b]

[a]*Department of Chemistry, Faculty of Science and Agriculture, University of the West Indies, St. Augustine, Trinidad and Tobago, West Indies;* [b]*Department of Chemistry, Faculty of Pure and Applied Sciences, University of the West Indies, Mona Campus, Kingston 7, Jamaica, West Indies*

(Received 5 January 2009; final form 23 February 2009)

The thermotropic phase behaviour of a homologous series of even chain length polymeric zinc(II) *n*-alkanoates, $Zn(C_nH_{2n-1}O_2)_2$ (ZnC_{4-20}) has been studied by means of differential scanning calorimetry (DSC) and temperature variation polarising light microscopy. The compounds exhibit both enantiotropic and monotropic phase behaviour on heating to the isotropic liquid and on cooling back to the room temperature solid, as seen from the following phase sequences: ZnC_{4-12}, Lamellar Crystal ↔ Crystal I ↔ Crystal II ↔ Isotropic Melt; ZnC_{14-16}, Lamellar Crystal ↔ Crystal I ↔ Isotropic Liquid; ZnC_{18-20}, Lamellar Crystal → Isotropic Liquid, Lamellar Crystal ← Smectic C ← Isotropic Liquid. The total enthalpy and entropy change for melting increase linearly with chain length and are higher than expected for complete fusion of alkyl chains suggesting that the step-wise melting process involves fusion of alkyl chains and changes in electrostatic interactions in the polar region of the molecule. The phase diagrams show that phase sequences for first and second heating cycles are almost indistinguishable, where the lamellar crystal is most stable for the long chain length homologues. In addition, there is a stable mesomorphic region over a narrow temperature range, at high temperatures for the long chain length compounds. Polymorphism is exhibited and is dependent on the method of preparation.

Keywords: zinc(II) *n*-alkanoates; thermotropic phase behaviour; differential scanning calorimetry; polarising light microscopy; step-wise melting process; smectic C mesophase; polymorphism

1. Introduction

Liquid crystalline phenomena are observed in a wide range of areas in the physical, biological and material sciences. Mesogenic behaviour is clearly a worthy topic of investigation owing to the wide range of technological applications, such as twisted nematic and ferroelectric display devices (*1*), wide-spread use of surfactants in the cleaning industry (*2*) and the importance of self-assembly in a large number of biological processes (*3*). In the last three decades there have been considerable advances in characterising the structures of various liquid crystalline phases and metal carboxylates have been at the forefront of this area of research. Several phase structures including lamellae, discs, rods and ribbons in various one-, two- and three-dimensional arrangements have been proposed for many metal carboxylates (*4*, *5*). Indeed, the phase behaviour of these carboxylates depends on both the metal and carboxylate chain length, but the assignment of many of the mesophases is often controversial and some of the proposed structures must be treated with caution.

For zinc(II) *n*-alkanoates, there have remained some unanswered questions regarding their phase sequences and phase structures. For example, Akanni *et al.* (*4*) in their review stated that zinc(II) soaps, on heating, passed directly from solid to liquid, without forming any intermediate phases. Nevertheless, the formation of a liquid crystalline phase has been suggested on cooling zinc(II) stearates from the melt (*4*). Furthermore, there are reports of the presence of various solid–solid phase transitions in the phase sequence for the short chain length adducts (*4*, *6*), although it is believed that such transitions were a result of the presence of impurities. Studies undertaken by Konkoly-Thege *et al.* (*6*) as well as Berkesi *et al.* (*7*) attempted to correlate phase behaviour with molecular structures. However, in both cases, the molecular and lattice structures for the series studied were not definitively known and insufficient data were presented on the phase behaviour on cooling from the isotropic liquid, as well as reheating and subsequent cooling. It is reasonable to suspect that there might be changes in coordination around the metal ion as well as some degree of chain disordering when the compounds were heated to the isotropic liquid. In light of this, there must be some plausible explanation of what may be occurring when the compounds go through various heating–cooling cycles and what are the structural and thermodynamic factors resulting thereby. Any study attempting to produce explanations in this regard must take into consideration the initial room temperature molecular and lattice structures of these compounds as a prerequisite

*Corresponding author. Email: richard.taylor@sta.uwi.edu

ISSN 0267-8292 print/ISSN 1366-5855 online

DOI: 10.1080/02678290902842594
http://www.informaworld.com

in understanding the phase behaviour of these systems. Studies using a combination of several techniques such as single-crystal and powder X-ray diffraction, infrared and solid state ^{13}C-NMR (nuclear magnetic resonance) spectroscopies as well as polarising light microscopy with conoscopy showed that all compounds within the series crystallised in a monoclinic crystal system and their structure consists of a three-dimensional polymeric layered network with sheets parallel to the (100) plane, in which tetrahedrally coordinated zinc(II) ions are connected by alkanoate bridges in a syn–anti arrangement along a layer plane (*8–10*). The hydrocarbon chains are in the fully extended all-*trans* conformation and are arranged in a tail-to-tail double bilayer for the short chain length homologues but a head-to-tail double interdigitated bilayer for the long chain length homologues.

In this study, the thermal behaviour of even chain length zinc(II) *n*-alkanoates, from the butanoate to eicosanoate inclusive are investigated by differential scanning calorimetry (DSC) and hot-stage polarising light microscopy. From the data, an attempt is made to correlate the thermal behaviour of the compounds with their previously proposed room-temperature lattice structures (*8*, *9*) and phase diagrams are constructed in order to establish a relationship between transition temperatures and the phases over the entire series giving some indication of the stability of respective phases.

2. Experimental details

The preparation, purification and confirmation of the purity of the even chain length zinc(II) *n*-alkanoates have been described previously (*8*, *9*).

The phase profiles of freshly prepared compounds were determined using a Mettler TC 10A Processor attached to a DSC 20 standard cell. Between 3 and 10 mg of ungrounded powder samples were sealed in standard aluminium crucibles and heat flow was recorded at a heating rate of 2.0 K min^{-1} between temperatures of 323 and 453 K in a heating–cooling–reheating–recooling cycle. Triplicate thermograms were recorded in air, using an empty aluminium crucible with pierced lid as a reference.

Phase textures were studied using an Olympus CH-2 hot-stage polarised-light microscope fitted with an Olympus PM-6 35 mm camera. Light exposure was measured using an Olympus EMM-7 photomicrographic exposure meter. For each run, crystalline samples were sandwiched between a microscope slide and coverslip and placed on the aluminium heating stage of the microscope fitted with a thermometer probe. The samples were heated up to 5 K above their melting points at a rate of 2.0 K min^{-1} by a Reichert–Jung heater. The phase textures on cooling were photographed. Before the series of runs the thermometer probe was calibrated using a series of organic standards and a calibration curve was constructed. Also, both the slide and coverslip used were pretreated with a solution of 10% polyvinyl acetate (PVA) to obtain good homeotropic textures.

3. Results and discussion

The phase transitions for $ZnC_{4–20}$, inclusive, over a temperature range of 323.0–443.0 K are shown in Figure 1. One or more endothermic phase transitions between the solid and isotropic liquid, for the entire series are observed on first heating. For example, in the case of $ZnC_{4–10}$, there are three endothermic transitions: room-temperature lamellar crystal (L_C) to phase I between 356.1 and 373.3 K; phase I to phase II between 377.8 and 395.4 K; and phase II to isotropic liquid between 408.4 and 428.6 K. For $ZnC_{12–14}$, there are two endothermic transitions: L_C to phase I at

Figure 1. DSC thermograms for the first heating cycle for $ZnC_{4–20}$.

376.2 and 383.8 K, and phase I to isotropic liquid at 405.9 and 404.8 K, respectively. For $ZnC_{16–20}$, there is only one endotherm between the solid and isotropic liquid, which occurs between 405.7 and 406.7 K. The first endotherm for the short chain length homologues, $ZnC_{4–10}$, with the exception of ZnC_6 are very small and suggest that the phase structures are only slightly altered in forming phase I. In addition, the second endotherm for $ZnC_{4–10}$ is approximately one-third the size of the final melting endotherm, again suggesting a partial retention of the prior structure.

On cooling from the isotropic liquid, one or more exothermic transitions are observed as shown in Figure 2. As in the heating cycle, there are distinct differences observed as chain length changes. For example, the short chain homologues, $ZnC_{4–12}$, have three exotherms: the isotropic liquid to phase II between 415.5 and 390.3 K; phase II to phase I between 374.9 and 365.6 K; and the phase I to the L_C between 347.1 and 389.2 K. In general, the phase I to L_C transitions are very small and inconsistent. In the case of $ZnC_{14–16}$, two exothermic transitions are observed: the isotropic liquid to phase I at 386.5 and 392.8 K and phase I to L_C at 350.8 and 382.0 K. One exotherm at 390.2 K is observed for ZnC_{18}. The transitions for ZnC_{20} are not reproducible and could not be determined from individual thermograms owing to the peaks being ill-defined. Also, the phase II to phase I exotherms for $ZnC_{8,}$ which are doublets, could not be separated, even at lower cooling rates. For $ZnC_{14–18}$, the exotherms after the isotropic to phase II or phase I exotherm are small and very close to the melting exotherm. In general, the phase II to phase I and phase I to L_C exotherms are very small and are likely to be the reverse transitions for the heating process. In addition, there is considerable supercooling, in the range of 12.0–18.4 K for almost the entire series suggesting that these are likely to be crystal-to-crystal rather than mesomorphic transitions.

Furthermore, the highly viscous birefingent phase textures observed on cooling into the phase, which are resistant to a sheer stress applied to the microscope slide for $ZnC_{4–16}$, indicate crystal to crystal phase transitions only, between the room-temperature solid and

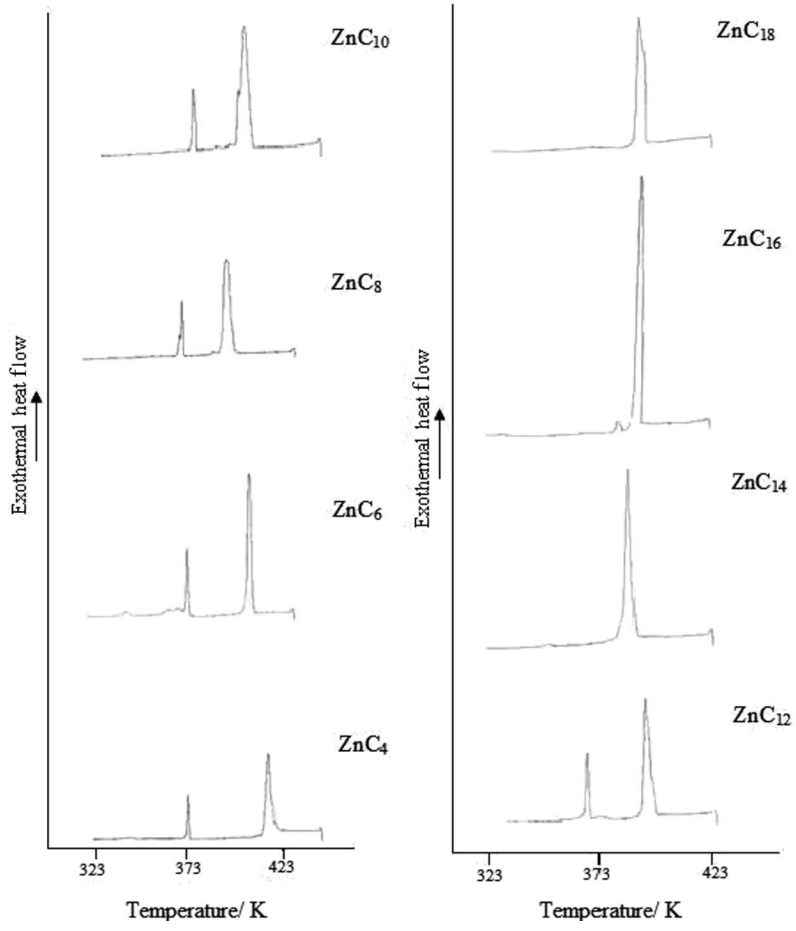

Figure 2. DSC thermograms for the first cooling cycle for $ZnC_{4–20}$.

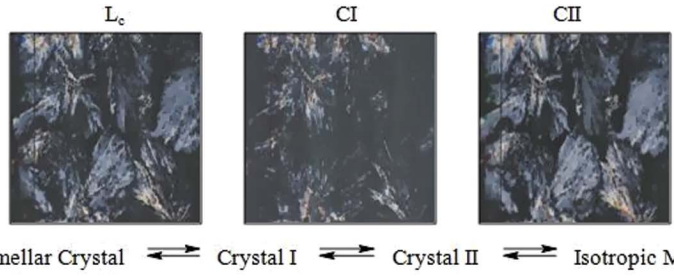

(a) Phase sequence for $ZnC_{4\text{-}12}$ for 1st heating – cooling cycle; ZnC_4, as an example.

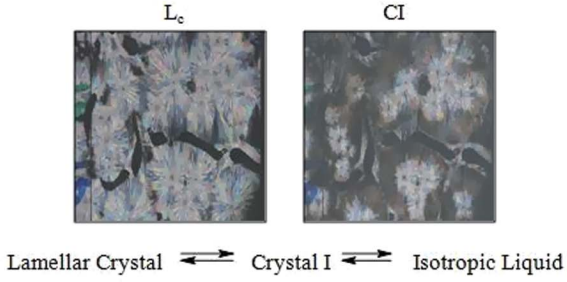

(b) Phase sequence for $ZnC_{14\text{-}16}$ for 1st heating – cooling cycle; ZnC_{16}, as an example.

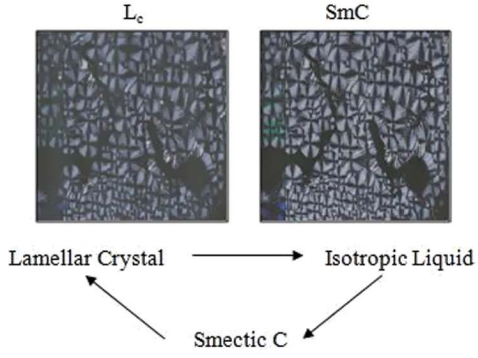

(c) Phase sequence for $ZnC_{18\text{-}20}$ for 1st heating – cooling cycle; ZnC_{18}, as example.

* The isotropic transitions are very dark and indistinctive and hence not shown.

Figure 3. Representative microscopic phase textures.

isotropic liquid, as reported previously (*6*). In addition, the brightly coloured radiating textures are typical for crystalline structures (Figure 3). The transitions are reversible, that is, they exhibit enantiotropic phase behaviour as shown in Figure 3(a) and (b). Interestingly, the long chain homologues, ZnC_{18} and ZnC_{20}, exhibit monotropic phase behaviour as shown Figure 3(c). This involves direct transition from the L_C to the isotropic melt on heating, but on cooling from the isotropic melt, a very fast, almost imperceptible transition to either a smectic C (SmC) or hexagonal phase is obtained, as seen from the broken fan textures which appeared on cooling into the phase. Since the short chain length compounds, from which suitable crystals were obtained for conoscopic studies gave biaxial interference figures for the room-temperature structures

indicating tilting of the hydrocarbon chains (*9*), support a SmC rather than hexagonal mesophase. Also, calculated tilt angles from X-ray data (*9*) for the series indicated that the chains were tilted. Indeed, a SmC phase consist of a tilted arrangement of the chains within the lamellae. The chains have some conformational disorder and slightly larger lateral distances leading to a higher area per carboxylate head group (*11*). The change back to the L_C at room temperature is very gradual and is probably kinetically controlled. Also, the crystal texture has retained many of the characteristics of the preceding smectic texture and looks more like a smectic phase than a crystalline phase, as posited by Neubert (*12*) for phase textures of other compounds. This demonstrates that transition from the isotropic melt to mesophase and crystal seems to be occurring almost simultaneously and could explain why these compounds also undergo supercooling.

The heated then cooled samples are immediately reheated and recooled at 2.0 K min^{-1} in order to check for reproducibility in DSC transition peaks. They are generally similar to those initially obtained on first heating, typified by ZnC_4 and ZnC_{18} shown in Figure 4. For instance, there are three endotherms for $ZnC_{4–12}$. However, for ZnC_6, three endotherms that could not be separated are observed in the vicinity of the L_C to phase I endotherm of the first heating cycle. The reason for the splitting of this endotherm is unclear. It could be that these new phases are metastable, arising from some subtle changes in the molecular lattice on reheating. Similar results were obtained with the lithium alkanoates (*13*). There are only two endotherms for ZnC_{14} and ZnC_{16}. The melting endotherm for ZnC_{18} is a doublet that could not be resolved even at lower heating rates. This could be a result of the almost simultaneous formation of the SmC and crystal phases. Also, the melting endotherm for ZnC_{20}, which has a shoulder, has a preceding exotherm. This observation is not unusual as premelting exotherms were observed by Vold *et al.* (*14*) in the thermograms for LiC_{16}. One possible reason is that there is a rearrangement of the structure arising from the formation of new bonds. In general, the transition temperatures are approximately the same between the first and second heating. On cooling a second time, one or more exotherms are observed for the series and are similar to those in the first cooling cycle as shown in

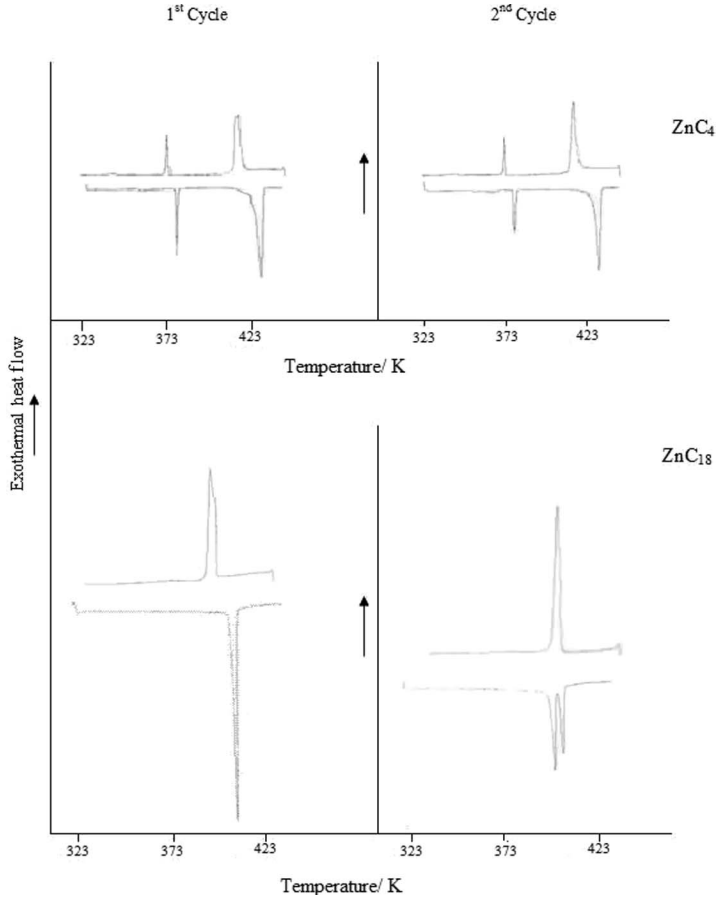

Figure 4. DSC thermograms for the first and second heating–cooling cycles of ZnC_4 and ZnC_{18}.

Figure 4. For $ZnC_{4–12}$ there are three endotherms; for $ZnC_{14–18}$, there are two. As in the first cooling cycle, the phase II to phase I and phase I to L_C transitions are small. There is considerable supercooling into each phase as before in the range of 10.4–14.7 K.

Transition temperatures, measured enthalpies of transition, $\Delta_{trans}H$, and calculated entropies of transition, $\Delta_{trans}S$, for the first heating cycle, are given in Table 1. The L_C phase to phase I transition, for $ZnC_{4–14}$ is fairly distinct and the corresponding $\Delta_{trans}H$ and $\Delta_{trans}S$ values are small, ranging from 2.89 to 13.69 kJ mol^{-1} and from 1.74 to 38.44 J K^{-1} mol^{-1}, respectively. They indicate very little structural change in going from the L_C phase to phase I, as confirmed by the similarity in the microscopic phase textures shown in Figure 3. These observations are similar to those by Konkoly-Thege *et al.* (*6*), where they reported that for the even chain homologues, $ZnC_{6–12}$, the first transition occurred from 353.0 to 373.0 K, with $\Delta_{trans}H$ ranging from 1.00 to 7.00 kJ mol^{-1}. The difference in $\Delta_{trans}H$ in both studies is attributed to the fact that in the previous study (*6*), calculations were based on the molecular formula of a monomer unit and not the molecular formula of the dimer unit determined from single-crystal analyses (*8*, *9*, *15*). Therefore, doubling of those values to represent the dimer units results in $\Delta_{trans}H$ ranging from 2.00 to 14.00 kJ mol^{-1} and thus are comparable to the values obtained in our case; there are no corresponding $\Delta_{trans}S$ values reported for this transition. The $\Delta_{trans}H$ and $\Delta_{trans}S$ values for the second endotherm, representing the phase I to phase II transition are also relatively small ranging from 9.81 to 21.51 kJ mol^{-1} and 25.87 to 54.39 J K^{-1} mol^{-1}, respectively. It is observed that the average value for the second transition is approximately twice as large as those of the first transition, possibly indicating a slight modification of the structure. Moreover, there is no trend with chain length for this transition. Again, these findings are similar to those reported in the literature (*6*). Indeed, a second transition, for $ZnC_{6–10}$, occurring with $\Delta_{trans}H$ ranging from 3.80 to 9.20 kJ mol^{-1} {(7.60–18.40) kJ mol^{-1}, corrected} was reported. The third transition, phase II to liquid transition (fusion), occurs between 405.1 and 428.6 K. The $\Delta_{fusion}H$ values range from 40.96 to 235.47 kJ mol^{-1} and $\Delta_{fusion}S$ from 95.57 to 578.98 J K^{-1} mol^{-1} and when plotted against chain length, n_c, result in reasonably good linear correlations as shown in Figure 5 (equations of line are shown on the graphs).

There is no previous report of thermodynamic data for the second heating cycle. However, in this case, the $\Delta_{trans}H$ and $\Delta_{trans}S$ values for these phase transitions are given in Table 2 and appear similar to the first heating cycle. The small values for the L_C to phase I transition for $ZnC_{4–14}$ and phase I to phase II transitions for $ZnC_{4–12}$ indicate very little structural change. For the melting transition, there is a decrease in temperature with increasing chain length and plots of $\Delta_{fusion}H$

Table 1. Thermodynamic data from the first and second heating cycles for even chain length zinc(II) *n*-alkanoates.

		Lamellar Crystal, L_C – Phase I			Phase I – Phase II			L_c/Phases I/II – Isotropic Liquid			Total	
Cycle	Compound	T/±0.9 K	$\Delta_{trans}H$/ ±0.14 kJ mol^{-1}	$\Delta_{trans}S$/ ±0.38 J K^{-1} mol^{-1}	T/±1.0 K	$\Delta_{trans}H$/ ±0.15 kJ mol^{-1}	$\Delta_{trans}S$/ ±0.39 J K^{-1} mol^{-1}	T/±1.0 K	$\Delta_{trans}H$/ ±1.13 kJ mol^{-1}	$\Delta_{trans}S$/ ±4.61 J K^{-1} mol^{-1}	$\Delta_{total}H$/ ±1.78 kJ mol^{-1}	$\Delta_{total}S$/ ±5.18 J K^{-1} mol^{-1}
1	ZnC_4	364.2	4.24	11.46	377.8	10.10	26.72	428.6	40.96	95.57	55.30	133.76
	ZnC_6	356.1	13.69	38.44	379.2	9.81	25.87	419.2	48.83	116.48	72.33	180.79
	ZnC_8	373.3	2.89	1.74	395.4	21.51	54.39	412.2	76.60	185.83	103.07	241.96
	ZnC_{10}	372.9	3.05	15.20	385.9	17.84	46.24	408.4	91.89	225.08	112.78	286.52
	ZnC_{12}	376.2	3.20	8.55	–	–	–	405.9	140.68	346.63	143.88	355.18
	ZnC_{14}	383.8	12.10	31.51	–	–	–	404.8	152.43	376.56	164.53	408.07
	ZnC_{16}	–	–	–	–	–	–	405.7	205.07	505.47	205.07	505.47
	ZnC_{18}	–	–	–	–	–	–	406.7	235.47	578.98	235.47	578.98
	ZnC_{20}	–	–	–	–	–	–	406.1	232.64	572.93	232.64	572.93
2	ZnC_4	356.1	2.08	5.85	377.3	9.53	25.27	429.0	45.87	106.92	57.49	138.04
	ZnC_6	366.9	1.55	4.22	378.0	11.51	30.45	418.8	47.42	113.22	60.48	147.89
	ZnC_8	378.5	10.03	26.49	386.4	4.80	12.43	411.3	72.65	176.66	87.48	215.58
	ZnC_{10}	372.3	11.17	30.00	384.7	4.53	11.77	408.3	81.93	200.69	97.63	242.46
	ZnC_{12}	366.7	16.70	45.56	375.0	5.21	13.88	405.2	99.49	245.56	121.40	305.00
	ZnC_{14}	381.7	6.39	16.74	–	–	–	402.6	111.19	276.18	117.58	292.92
	ZnC_{16}	–	–	–	–	–	–	403.3	164.72	408.48	164.72	408.48
	ZnC_{18}	–	–	–	–	–	–	401.1	171.78	428.27	171.78	428.27
	ZnC_{20}	–	–	–	–	–	–	403.9	205.07	507.79	205.07	507.79

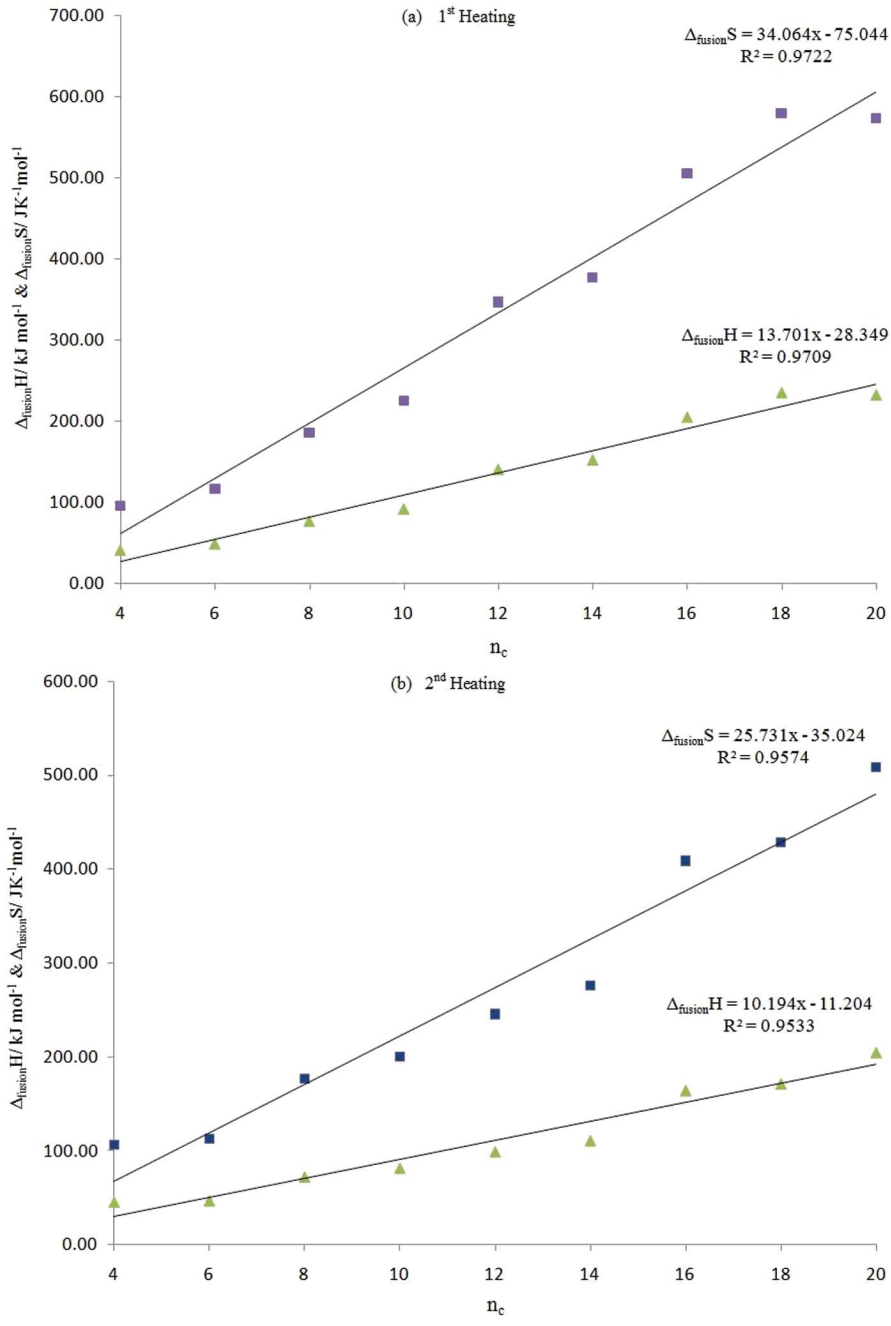

Figure 5. Plots of $\Delta_{fusion}H$ and $\Delta_{fusion}S$ versus n_c for (a) first and (b) second heating cycles for ZnC_{4-20}.

and $\Delta_{fusion}S$ values versus n_c, result in reasonably good linear correlations as shown in Figure 5. Overall, the values in the second heating cycle are slightly smaller than those in the first cycle and could be attributed to the formation of metastable phases on first cooling. Clearly, there appears to be some subtle modification of the molecular structure after heating and subsequent cooling, as seen from slight changes in the microscopic phase textures (for ZnC_4 and ZnC_{18} as examples) between first and second cooling, as shown in Figure 6.

Similarly, there is no previous report of thermodynamic data from the first and second cooling cycles given in Table 2 in this case. For the first cycle, the isotropic liquid to phase II transition temperatures are very similar and decrease with increasing n_c. However, the decrease is less dramatic when compared with the heating cycle. On the other hand, the $\Delta_{trans}H$ and $\Delta_{trans}S$ values for this transition increase with increasing n_c and range from 41.19 to 173.99 kJ mol^{-1} and from 99.15 to 445.96 J K^{-1} mol^{-1}, respectively. Plots of $\Delta_{trans}H$ and $\Delta_{trans}S$ values against n_c result in

Table 2. Thermodynamic data from the first and second cooling cycles for even chain length zinc(II) *n*-alkanoates.

		Phase II – Phase I			Isotropic Liquid – Phase II			Total	
Cycle	Compound	$T/\pm0.6$ K	$\Delta_{trans}H/\pm0.19$ kJ mol^{-1}	$\Delta_{trans}S/\pm0.51$ J K^{-1} mol^{-1}	$T/\pm0.7$ K	$\Delta_{trans}H/\pm1.55$ kJ mol^{-1}	$\Delta_{trans}S/\pm4.02$ J K^{-1} mol^{-1}	$\Delta_{total}H/\pm1.80$ kJ mol^{-1}	$\Delta_{total}S/\pm4.49$ J K^{-1} mol^{-1}
1	ZnC_4	374.4	8.27	22.09	415.5	41.19	99.15	49.46	148.61
	ZnC_6	374.9	17.63	47.03	405.7	48.18	118.77	65.81	184.58
	ZnC_8	375.7	14.65	39.00	399.2	68.63	171.94	83.28	255.22
	ZnC_{10}	370.3	13.50	36.46	396.4	80.63	203.43	94.13	297.56
	ZnC_{12}	365.6	29.33	80.22	390.3	100.43	257.35	129.76	387.11
	ZnC_{14}	350.8	24.43	69.65	386.5	125.80	325.53	150.23	475.76
	ZnC_{16}	382.0	5.37	14.06	392.5	168.27	428.71	173.64	602.35
	ZnC_{18}	–	–	–	390.2	173.99	445.96	173.99	619.95
	ZnC_{20}	–	–	–	–	–	–	–	–
2	ZnC_4	374.3	7.86	21.00	415.1	40.76	98.21	48.62	119.21
	ZnC_6	371.7	17.73	47.71	404.1	48.75	120.64	66.48	168.34
	ZnC_8	375.5	13.83	36.83	399.6	67.18	168.14	81.01	204.97
	ZnC_{10}	370.3	13.84	37.38	397.1	80.01	201.49	93.85	238.86
	ZnC_{12}	365.5	26.51	72.53	394.2	96.11	243.84	122.62	316.37
	ZnC_{14}	352.5	2.41	6.84	388.8	112.85	290.29	115.26	297.13
	ZnC_{16}	382.2	6.33	16.56	392.9	156.21	397.63	162.54	414.20
	ZnC_{18}	–	–	–	390.7	173.64	444.49	173.64	444.49
	ZnC_{20}	–	–	–	–	–	–	–	–

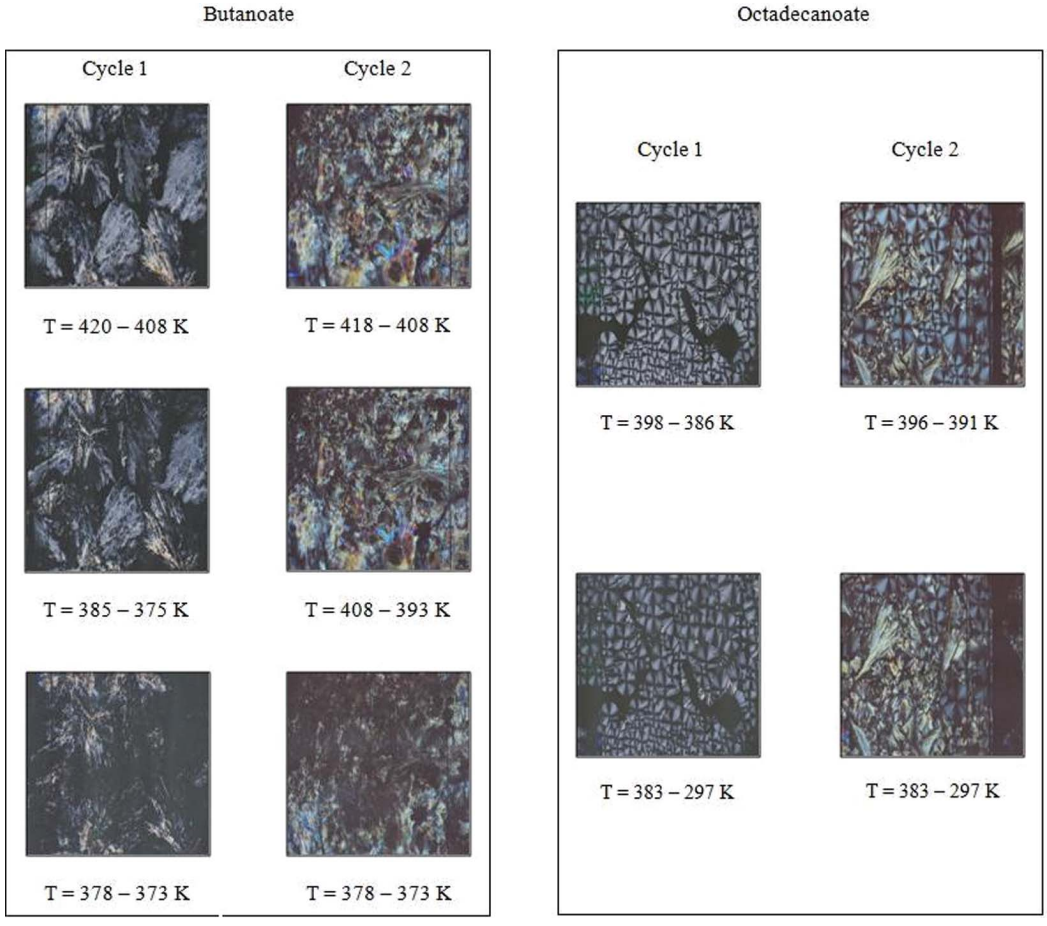

Figure 6. Microscopic phase textures of ZnC_4 and ZnC_{18}; slight differences between first and second cycles.

Table 3. Calculated values for slope and intercept from linear plots of ΔH and ΔS versus n_c for heating and cooling cycles.

Run	Cycle	Type of graph	Slope	Intercept	Reference
		$\Delta_{fusion}H$	13.14	–25.14	(*6*)
		$\Delta_{fusion}H$	7.62	10.44	(*7*)
	First	$\Delta_{fusion}H$	13.70	–28.35	This study
Heating	Second	$\Delta_{fusion}H$	10.19	–11.20	This study
	First	$\Delta_{total}H$	12.12	1.77	This study
	Second	$\Delta_{total}H$	9.16	10.54	This study
		$\Delta_{fusion}S$	32.96	–70.13	(*6*)
		$\Delta_{fusion}S$	19.93	16.63	(*7*)
	First	$\Delta_{fusion}S$	34.06	–75.04	This study
Heating	Second	$\Delta_{fusion}S$	25.73	–35.02	This study
	First	$\Delta_{total}S$	30.00	2.65	This study
	Second	$\Delta_{total}S$	22.97	22.85	This study
	First	$\Delta_{trans}H$	10.25	–11.82	This study
Cooling	Second	$\Delta_{trans}H$	9.65	–9.17	This study
	First	$\Delta_{trans}S$	26.74	–37.77	This study
	Second	$\Delta_{trans}S$	25.11	–30.57	This study

reasonably good linear correlations; the resulting slope and intercept values are given in Table 3. For the phase II to phase I transition, the $\Delta_{trans}H$ and $\Delta_{trans}S$ values are much smaller than the previous transition and show no trend with n_c. They range from 5.37 to 29.33 kJ mol^{-1} and from 14.06 to 80.22 J K^{-1} mol^{-1}, respectively. The phase I to L_C transitions values are very small and irreproducible and hence not reported. For the second cycle the data are similar to those from the first cooling cycle. The isotropic liquid to phase II transition temperatures decrease with increasing n_c and the $\Delta_{trans}H$ and $\Delta_{trans}S$ values for this transition increase with increasing n_c; the slope and intercept values from linear plots are given in Table 3.

In addition, plots of $\Delta_{total}H$ and $\Delta_{total}S$ with n_c for each heating cycle also result in reasonably good linear correlations and the resulting slope and intercept values are tabulated in Table 3 and compared with values from $\Delta_{fusion}H$ and $\Delta_{fusion}S$ plots from the literature (*6*, *7*). The linear dependence of $\Delta_{fusion}H$, $\Delta_{fusion}S$, $\Delta_{total}H$ and $\Delta_{total}S$ with n_c for the melting process can be interpreted on the basis of a simple model, taking into consideration interactions between neighbouring alkyl chains as a function of the number of CH_2 groups in the chain and also corresponding changes in the polar head groups involving interaction between the carboxyl group and zinc ion (COO–Zn). It is not unreasonable to assume, in view of the fact that the chains are arranged in an all-*trans* conformation, in layered sheets (*9*), that the interactions in the tail groups are constant during fusion and, hence,

$$\Delta_{fusion}H[Zn\{O_2C(CH_2)_nCH_3\}_2] = n\Delta_{fusion}H(CH_2) + \Delta_{fusion}H[CH_3^- + (CO_2)_2Zn].$$

The slopes of the lines indicate the contribution from a single CH_2 group to the inter-chain interactions and the intercepts, the enthalpies of rearrangement of the bonds between the zinc(II) ion and the COO^- groups and also the terminal CH_3 groups in the molecular structure. The entropy contribution can be expressed similarly.

For the first heating cycle, slopes from $\Delta_{fusion}H$ plots of 13.70 kJ mol^{-1} ($\Delta_{total}H$; 12.12 kJ mol^{-1}) indicate that the major process during melting is the stepwise disordering of the hydrocarbon chains in the crystal lattice. These values compare well with 13.14 kJ mol^{-1} reported by Konkoly-Thege *et al.* (*6*) but different from that by Berkesi *et al.* (*7*) who obtained a value of 7.62 kJ mol^{-1}. It could be that the compounds prepared by Berkesi *et al.* (*7*) were structurally different; that is, polymorphic structures were produced, depending on the method of preparation or they were impure. Indeed, the compounds studied by Konkoly-Thege *et al.* (*6*) were prepared by metathesis in alcoholic solution using potassium carboxylate and zinc nitrate and those by Berkesi *et al.* (*7*) from the neutralisation of carboxylic acid with zinc hydroxide. The differences in these compounds were seen in the visual melting points, where in the latter, they were generally slightly higher and could suggest greater purity. For both sets of compounds, the results of elemental analyses and infrared spectroscopy indicated that they were free from impurities and hence the difference in melting points is likely to be as a result of polymorphism in which the compounds have slightly different arrangements of the hydrocarbon chains in the crystal lattice. Indeed, Berkesi *et al.* (*7*) stated that their compounds crystallised in a triclinic crystal system and not monoclinic as observed for our compounds (*8*, *9*). Polymorphism for some short chain zinc(II) *n*-alkanoates were also reported by Šegedin *et al.* (*16*), where different preparative methods were suggested to be the reason for this observation.

In addition, for metal carboxylates, the enthalpy change associated with the fusion process can be decomposed based on energy contributions as follows (*17*, *18*):

$$\Delta_{fusion}H = \Delta U_{conf} + \Delta U_{vdW} + \Delta U_o + p\Delta V, \quad (2)$$

where: ΔU_{conf} and ΔU_{vdW} are energy changes associated with intramolecular conformational disorder (that is, introduction of gauche conformations in the chains during melting) and intermolecular van der Waals interactions, respectively; ΔU_o incorporates all other energy changes, such as electrostatic interactions; and $p\Delta V$, the energy associated with changes in the molar volume, is small compared with the others and can be neglected. The linear increase in the overall

enthalpy of fusion with n_c is associated with both the decrease in the van der Waals interactions between the hydrocarbon chains and introduction of some degree of conformational disorder (*17–19*). A value for the slope of the plot of $\Delta_{fusion}H$ versus n_c of 13.70 kJ mol^{-1} per CH_2 is almost twice as large as the value of 7.60 kJ mol^{-1} per CH_2 obtained from complete fusion of the aliphatic chains from their fully crystalline dimeric state of carboxylic acids(3.80 kJ mol^{-1} per CH_2 for the monomer unit) (*20*). Furthermore, from $\Delta_{fusion}S$ versus n_c plots, a value of the slope of 34.06 J K^{-1} mol^{-1} per CH_2 ($\Delta_{fusion}S$; 30.00 J K^{-1} mol^{-1}) is considerably higher than 19.86 J K^{-1} mol^{-1} per CH_2 for complete fusion of aliphatic chains for the dimeric parent acid (9.93 J K^{-1} mol^{-1} per CH_2 for monomer unit) (*20*). This suggests that the chains are fully fused and there is a very high degree of conformational disorder where the orientation of the CH_2 groups of the chains has changed from all-*trans* to a high degree of gauche conformation. Since the chains are fully fused, it suggests that the melt is totally disordered. This is not in accord with what was observed for other metal carboxylates such as lead(II) (*17*) and cadmium(II) (*6*) where a small degree of aggregation of the molecules in the melt was suggested.

Furthermore, extrapolation to zero CH_2 groups of the $\Delta_{fusion}H$ plots gives an intercept value of –28.35 kJ mol^{-1}, which implies that electrostatic interactions give a fairly strong negative contribution to the fusion process. This is similar to the even chain length series of cerium(III) octanoate–octadecanoate inclusive, where Marques *et al.* (*18*) found an intercept value of –49.0 kJ per CH_2 which they attributed to electrostatic interactions. They suggested that when the compounds melted, repulsive electrostatic interactions between the cerium trivalent ions were reduced, leading to a stabilisation of the system. Also, lateral relaxation of the lattice may be accompanied by a longitudinal change at the polar head groups. Indeed, there may be some fusion of the polar region leading to a perturbation of the metal carboxylate interaction. Similar results were obtained for the even chain length mercury(II) carboxylates (*21*). Interestingly, Konkoly-Thege *et al.* (*6*) obtained a value of –25.15 kJ mol^{-1} for their compounds in contrast to 10.54 kJ mol^{-1} for those of Berkesi *et al.* (*7*). This difference is not surprising, as Berkesi *et al.*'s compounds are considered to be different polymorphs or may be hydrated. The positive intercept may be attributed to the fact that part of the enthalpy change is a result of the loss of water of hydration in the lattice which overwhelms the negative contribution owing to electrostatic interactions as was proposed for neodymium(III) alkanoates (*22*). Clearly, the compounds studied by Konkoly-Thege *et al.* (*6*) may have a similar lattice arrangement to our compounds.

Interestingly, the linear trends obtained from plots of $\Delta_{fusion}H$ and $\Delta_{fusion}S$ (and also $\Delta_{total}H$ and $\Delta_{total}S$, not included) against n_c, using the present data, are different from what were observed previously, although this is not surprising. Two sets of lines with different intercepts were observed for $\Delta_{fusion}H$ and $\Delta_{fusion}S$ plots for short chains, n_c = 6, 8, 10, and medium–long chains, n_c = 12, 14, 16, 18 (see (*7*)). The authors attributed this to structural differences in the COO–Zn portion of the molecule; the interactions of the hydrocarbon chains were suggested to be nearly the same in both cases. In the case here, it is important to note that there is no apparent difference in the melting behaviour as seen from the $\Delta_{fusion}H$ and $\Delta_{fusion}S$ (and also $\Delta_{total}H$ and $\Delta_{total}S$) plots between short and long chain homologues, even though the arrangement of the hydrocarbon chains is lamellar bilayer for the short chain homologues and interdigitated bilayer for the longer chain homologues. Our previously proposed (*9*) structural models suggest that the CH_2 groups of the tilted hydrocarbon chains are oriented in a similar manner in parallel sheets; that is, they have all-*trans* arrangement with inter-grooving between chains in both types of lamellae and therefore the way in which the chains melt would be the same in both cases.

The large $\Delta_{fusion}H$ and $\Delta_{fusion}S$ (and also $\Delta_{total}H$ and $\Delta_{total}S$) values indicate that the hydrocarbon chains have completely collapsed and there is little or no formation of micellar aggregates at or after melting. Nevertheless, it is possible there is some structural deformation of the polar head groups during melting. Observation of the cooling and reheating cycles from DSC measurements should provide some insight into the reversibility and stability of the various phases, thereby giving an indication of possible changes in COO–Zn coordination. Since the thermodynamic data of the melting transition obtained from the second cycle are almost similar to those from the first cycle; although in the latter case the values are somewhat lower, this suggests that on first heating and subsequent cooling, the compounds return to a room-temperature molecular structure not very different from the original structure. Indeed, the microscopic phase textures shown in Figure 6 for ZnC_4 and ZnC_{18} for the first and second cooling cycles suggest that the structures are only slightly different after heating–cooling–reheating. Similarity in the slope and intercept values from linear plots (Table 3) for corresponding heating and cooling cycles indicate that they are fairly reversible, even though there may be some slight modification of the structure, as reflected in slight differences in the values.

The phase diagrams of transition temperature versus n_c in Figure 7 for both first and second cycles,

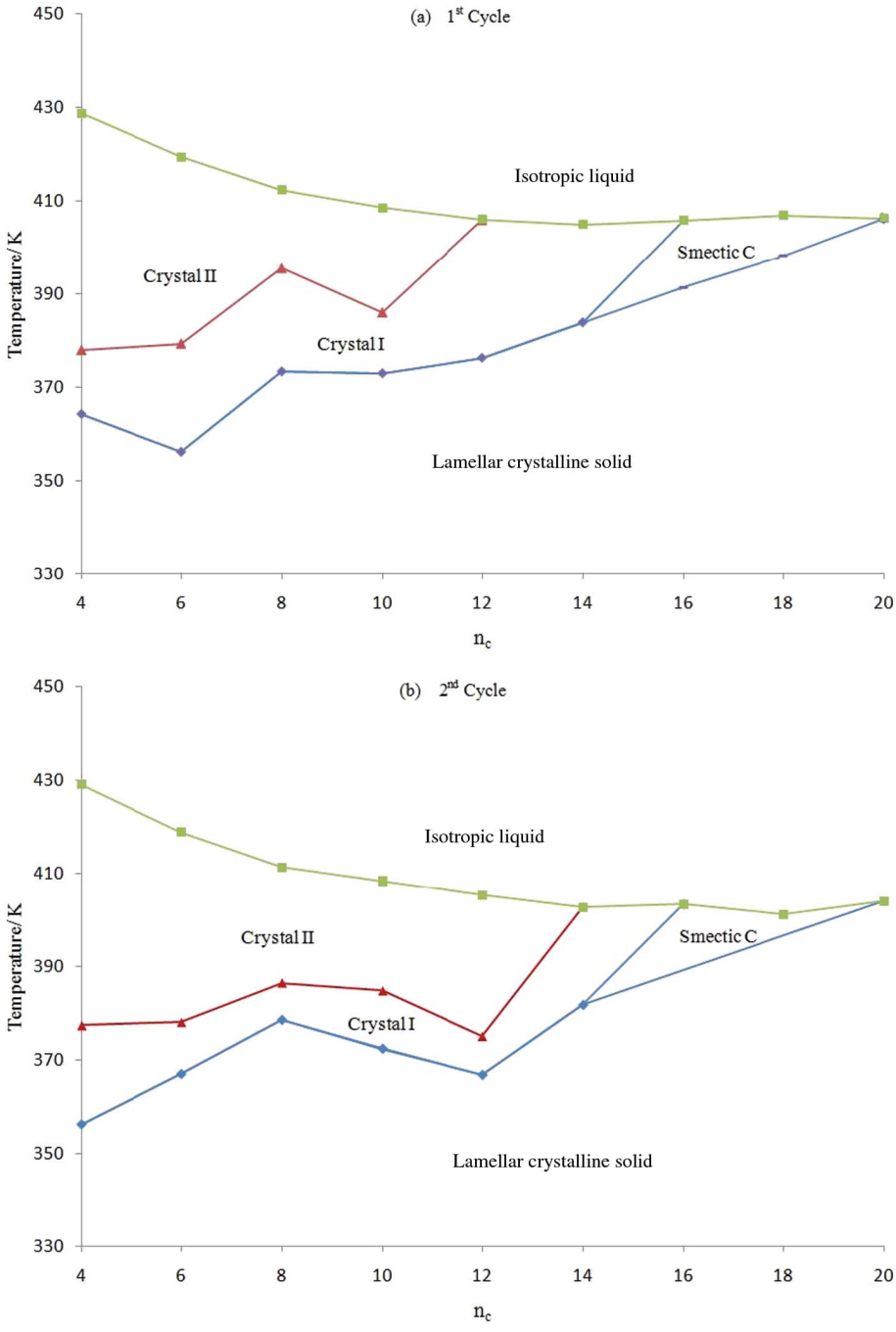

Figure 7. Phase diagrams of even chain length $ZnC_{4–20}$ for (a) first and (b) second heating cycles.

respectively, show that the phase sequences for both cycles are almost imperceptible and reflect the relationship of the number and type of phase(s) with chain length. From the phase diagrams, it can be seen that the lamellar crystal is most stable for the longer chain length homologues because the number of transitions are fewer than the short chain length homologues. The increased stability is a result of the higher order of the lattice structure arising from the interdigitated arrangement of the hydrocarbon chains. This trend also indicates that interdigitation increases with n_c. Here, the entropy of the lattice structure decreases with n_c and therefore requires more energy to transform it into an isotropic melt. However, the fusion temperatures decrease with n_c up to the point at which interdigitation predominates. It seems that the higher order of the crystal lattice for the longer chain homologues prevents them from going through

various, subtle lattice modifications, prior to the lattice structure collapsing into the more disordered, non-micellar isotropic melt. It can be assumed that the higher order of the crystal lattice network is as a result of both an increase in the van der Waals interactions between hydrocarbon chains which increase with n_c and the decrease in the repulsive interactions between the zinc basal planes. In addition, as interdigitation predominates, the interaction between the terminal CH_3 group and COO–Zn polar region becomes slightly more significant for the longer chain homologues and therefore offers some degree of stability for the lattice. As the structure reorganises on cooling, from the disordered isotropic melt, the interaction between CH_3 group and COO–Zn polar region, along with the van der Waals interactions influence the formation of the smectic mesophase for the longer chain homologues. For the medium chain homologues for which the interaction between the terminal CH_3 and COO–Zn is not appreciable and the shorter chain homologues for which it is absent, the van der Waals forces are not large enough to influence the formation of these mesophases. The formation of mesophases as the compound cools from the isotropic liquid is also indicative of the higher degree of order of the crystal lattice for the longer chain homologues.

4. Conclusion

A combination of DSC data and microscopic phase textures indicate that a homologous series of even chain length zinc(II) *n*-alkanoates from the butanoate to eicosanoate inclusive display both enantiotropic and monotropic phase behaviour. There is some relationship with the number of phases observed with chain length; there are three transitions for the short chain, two for the medium chain and one for the long chain homologues. These are ascribed to possible difference in lattice structures of the starting material. On heating the short and medium chain length compounds, only solid-to-solid transitions occur, but, interestingly, on cooling from the isotropic melt, a SmC mesophase appears for the long chain length octadecanoate and eicosanoate. Since the smectic textures for the long chain length homologues persist at room temperature, they appear to be kinetically controlled. Enthalpy and entropy change for fusion suggest that electrostatic interactions in the polar region play an important role in the melting process along with fusion of the hydrocarbon chains being the major part, leading to an isotropic melt with very few or no micellar aggregates. The phase diagrams show that the lamellar crystal is most stable for the longer chain length homologues and for these there is the presence of a SmC phase which is stable over a very narrow temperature range.

Acknowledgement

The authors express thanks to the School for Graduate Studies and Research of the University of the West Indies, Mona, for funding this research.

References

(1) Bruce, D.W. *J. Chem. Soc., Dalton Trans.* **1993**, 1983–1989.
(2) Engels, T.; von Rybinski, W. *J. Mater. Chem*. **1998**, *8*, 1313–1320.
(3) Corkery, R.W. *Phys. Chem. Chem. Phys*. **2004**, *6*, 1534–1546.
(4) Akanni, M.S.; Okoh, E.K.; Burrows, H.D.; Ellis, H.A. *Thermochim. Acta* **1992**, *208*, 1–41.
(5) Polishchuk, A.P.; Timofeeva, T.V. *Russ. Chem. Rev*. **1993**, *62*, 291–321.
(6) Konkoly-Thege, I.; Ruff, I.; Adeosun, S. O.; Sime, S. J. *Thermochim. Acta* **1978**, *24*, 89–96.
(7) Berkesi, O.; Katona, T.; Dreveni, I.; Andor, J. A.; Mink, J. *Vib. Spect.* **1995**, *8*, 167–174.
(8) Taylor, R.A.; Ellis, H.A.; Maragh, P.T.; White, N.A.S. *J. Mol. Struct.* **2006**, *787*, 113–120.
(9) Taylor, R.A.; Ellis, H.A. *Spectrochim. Acta* **2007**, *68*, 99–107.
(10) Taylor, R.A.; Ellis, H.A. *J. Mol. Struct*. **2009**, *921*, 118–125.
(11) Demus, D.; Richter, L. *Textures of Liquid Crystals*; Verlag Chemie: New York, 1978.
(12) Neubert, M.E. *Identification of Liquid Crystal Textures*; Liquid Crystal Institute, Kent State University: Kent, OH.
(13) Skoda, W. *J. Colloid Polym. Sci*. **1969**, *234*, 1128–1134.
(14) Vold, M.J.; Funakoshi, H.; Vold, R.D. *J. Phys. Chem*. **1976**, *80*, 1753–1761.
(15) Taylor, R.A; Ellis, H.A. *Acta Cryst. E* **2008**, *E64*, m895.
(16) Šegedin, P.; Lah, N.; Žefran, M.; Leban I.; Golič, L. *Acta Chim. Slov*. **1999**, *46*, 173.
(17) Burrows, H.D. *The Structure, Dynamics and Equilibrium Properties of Colloidal Systems*; Kluwer: Dordrecht, 1990; pp. 415–426.
(18) Marques, E.F.; Burrows, H.D.; da Graça Miguel, M. *J. Chem. Soc., Faraday Trans*. **1998**, *94*, 1729–1736.
(19) Nagle, J.F. *Ann. Rev. Phys. Chem.* **1980**, *31*, 157–195.
(20) NIST Standard Reference Database, *NIST Chemistry Web-book 69*, 2005, http://webbook.nist.gov/chemistry/form-ser.html
(21) Shiba, S. *Railway Tech. Res. Inst. Rep.* **1961**, *34*, 804–809.
(22) Binnemans, K.; Jongen, L; Bromant, C.; Hinz, D.; Meyer, G. *Inorg. Chem.* **2000**, *39*, 5938–5945.